Uptake and Translocation Mechanisms of Cationic Amino Derivatives Functionalized on Pristine C_{60} by Lipid Membranes: A Molecular Dynamics Simulation Study

Sebastian Kraszewski,[†,*] Mounir Tarek,[‡,*] and Christophe Ramseyer[†]

[†]Laboratoire de Nanomédecine, Imagerie et Thérapeuthique, Université de Franche-Comté, Centre Hospitalier Universitaire de Besançon, 25000 Besançon, France and, [‡]UMR Structure et Réactivité des Systèmes Moléculaires Complexes, CNRS Nancy Université, France

ABSTRACT Bioactive molecules, cationic peptides among them, are nowadays well-recognized in modern pharmacology for their drug potential. However, they usually suffer from poor translocation across cell membranes, and specific drug carriers should be designed to circumvent this problem. In the present study, the uptake mechanism of fullerene bearing cationic ammonium groups by membranes modeled as lipid bilayers is investigated using extensive molecular dynamics simulations and free-energy calculations. Three main results issued from this work can be drawn. First, the fullerene core appears to be a good drug vector since it greatly enhances the uptake of the cationic groups by the membrane. Second, we show that the amino derivatives should be deprotonated at the lipid headgroup level in order to fully translocate the membrane by passive diffusion. Finally, the fullerenes bearing too many cationic groups display mostly a hydrophilic character; thus, the lipophilic fullerene core is not anymore effective as an insertion enhancer. Therefore, the lipid bilayer appears to be very selective with respect to the amount of amino groups conjugated with C_{60}.

KEYWORDS: fullerenes · cationic functionalization · drug vectors · uptake passive diffusion · molecular dynamics · free-energy profiles

Nanomedicine, a combinatorial approach using nanotechnology and medicine, has become an increasingly important field of research for diagnostics and theranostics.[1−3] The field of nanomedicine involves the design and development of novel nanomaterials such as multifunctional liposomal nanoparticles,[4−6] polymeric micelles,[7] iron oxide nanoparticles,[8] nanoshells,[9] and functionalized nanomaterials such as nanotubes[10,11] and fullerenes.[12−15] The latter, and more especially Buckminsterfullerenes (C_{60}), have unique physical and chemical properties.[16] Their nanometer size makes them perfectly suitable for biomedical applications. However, it is important to emphasize that their potential biological benefits can be fully realized only after chemical modifications. Indeed, C_{60}, like all carbon-based nanomaterials, has a poor solubility (less than 0.1 ng·L^{-1}) and displays a tendency for aggregation.[17,18] Accordingly, various functionalizations have been used to increase its hydrophilicity (*e.g.*, −OH, −COOH, $-NH_2$).[16] For instance, a very high level of solubility in water (34 mg·L^{-1}) can be obtained at pH = 7.4 with a dendritic fullerene containing up to 18 carboxylic groups.[12] The fullerene physical and chemical properties play critical roles in many biological processes. Their hydrophobicity and lipophilicity seem to be crucial in optimizing the interaction with the active site of various enzymes,[19,20] especially HIV proteases.[21,22] This specific character allows also C_{60} to directly intercalate into biological membranes, provoking destabilization,[23,24] and has an important role in the antibacterial activity found for several derivatives.[25−27]

Functionalization of fullerenes aimed at drug delivery application is another very active field of research (see recent review by Partha and Conyers).[15] Indeed, bioactive molecules, especially charged ones, belong to a major drugs class used in modern pharmacology, and there is a crucial need to enhance their translocations into cell membranes. For a wide variety of peptides, carbon nanomaterials such as nanotubes and fullerenes appear as effective drug carriers once grafting of peptide to the nanomaterial is achieved. Amphifullerenes, for example, which contain both hydrophobic and hydrophilic moieties, and their associated supramolecular complexes, known as "buckysomes", are very promising nanovectors that can deliver drug to specific sites.[28] Carboxyfullerenes, engineered with three malonic acid molecules, were also shown to be effective radical scavengers and to act *in vitro* and *in vivo* as neuroprotective antioxidants.[29] The relative toxicity of fullerene-based nanoparticles is

* Address correspondence to sebastian.kraszewski@univ-fcomte.fr; mounir.tarek@srsmc.uhp-nancy.fr.

Received for review May 27, 2011 and accepted October 7, 2011.

Published online October 07, 2011
10.1021/nn201952c

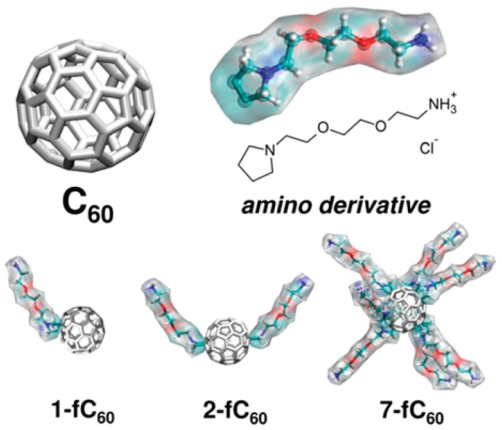

Figure 1. Neat C_{60}- and *n*-fC_{60}-functionalized fullerenes with *n* = 1, 2, or 7 amino derivatives investigated in this study.

mostly attributed to the ratio of the amphiphilic/lipophilic character of these derivatives, which can lead to cell membrane disruption and subsequent cellular death, as already observed in water-soluble C_{60} derivatives.[30] Note that, generally, monofunctionalized derivatives show only a moderate toxicity in comparison to more cytotoxic multifunctionalized compounds.[31]

Despite this widespread effective and potential use, only few studies have been devoted to characterize the molecular mechanisms of functionalized C_{60} (fC_{60}) cellular uptake. Almost all of them concerned theoretical investigations using all-atom or coarse-grained molecular dynamics (MD) simulations of neat C_{60} interacting with model membranes. Only one functionalization of the type $(OH)_n$ was the subject of studies addressing the issues of translocation of $C_{60}(OH)_{20}$ from water toward a dipalmitoyl-phosphatidylcholine (DPPC) bilayer hydrophobic core.[32,33] It was shown using unconstrained MD simulations that neat fullerene and its $(OH)_n$ (with $n \leq 10$) derivatives can easily "jump" into the bilayer and translocate into the membrane, while $C_{60}(OH)_{20}$ remains in the aqueous phase. In contrast to these bare compounds uptake, another mode of nanoparticle insertion into lipid bilayers has been recently studied using coarse-grained MD simulations. It involves precoating negatively charged nanocapsules with detergent and lipid molecules and fusion of the resulting liposome-like structure into a lipid membrane.[34]

Expanding on these pioneering studies, we use here extensive MD simulations aimed at characterizing the interaction of C_{60} and associated cationic functionalization groups with a lipid bilayer. We investigate, in particular, the uptake mechanism of a charged amino derivative ($CCNCCOCCOCCNH_3^+$) currently used for carbon nanostructure cell internalization.[35−38] The main goal of this paper is to shed light on the relative role of the fullerene core and functionalization groups

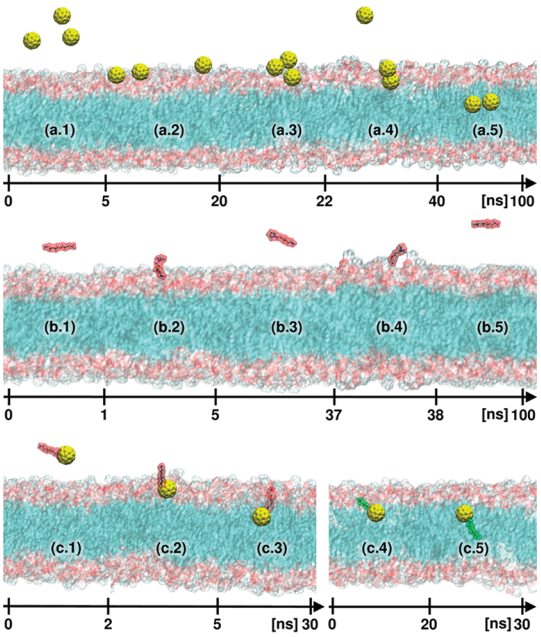

Figure 2. Uptake of a neat C_{60} (a), single cationic molecule (b), and 1-fC_{60} molecule (c) (monomeric cationic group conjugated to fullerene) by a POPC membrane. Results come from unconstrained MD simulations. In the case of C_{60} placed near the membrane (a.1), molecules go first on the membrane surface (a.2) and then start to aggregate (a.3). Aggregation seems to favors penetration (a.4), and the molecules translocate to hydrophobic tails (a.5). The positively charged amino derivative placed near the membrane (b.1) stays most of the time in the solution (b.3, b.5), reaching the membrane surface only during short periods of time (b.2, b.4). The cationic molecule sometimes perturbs the membrane surface (b.4); however, the uptake was not observed. In the case of 1-fC_{60} placed near the membrane (c.1) the molecule easily crosses the lipid headgroup region (c.2). However, due to strong interactions with lipid heads, it remains near the negatively charged phosphorus (c.3) and needs to be deprotonated (c.4) (see details in the text) before further translocation (c.5). The yellow balls indicate the fullerene core. The red transparent and elongated surface corresponds to the ionized cationic group, while the green one is its neutral form. The lipid membrane headgroup and tail sections are shown as red and blue surfaces, respectively. For clarity reasons, water molecules and other fullerenes or monoadducts that are not taken up are not shown.

on the uptake mechanism. Accordingly, we have investigated various systems comprising neat fullerenes and fC_{60} functionalized with one, two, and seven amino groups (see Figure 1). Obtained results show that the hydrophobic fullerene core is able to enhance membrane insertion of a reasonable amount of cationic residues.

RESULTS AND DISCUSSION

C_{60} Favors the Uptake of the Cationic Molecule by the Lipid Bilayer. Unbiased MD simulations show that monomeric neat fullerenes placed in bulk water next to a palmitoyl-oleyl-phosphatidyl-choline (POPC) model lipid membrane spontaneously enter the bilayer within the hundred nanosecond time scale (see Figure 2a). Fullerene crosses the lipid headgroup region (after

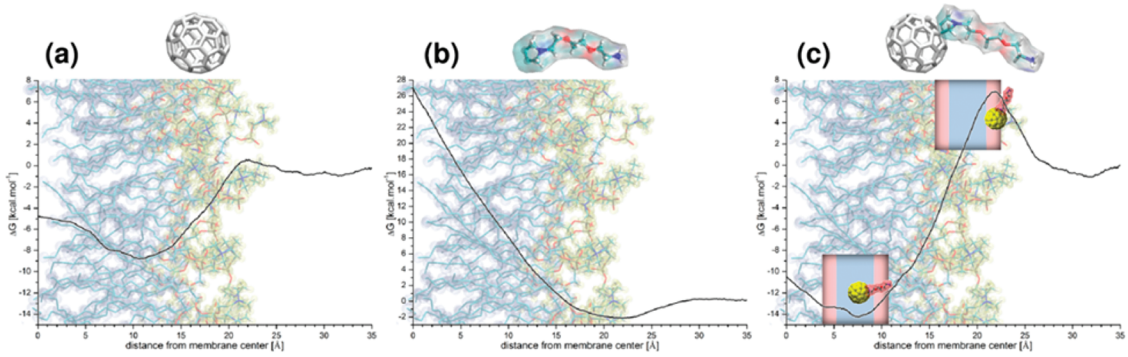

Figure 3. Free-energy profile of translocation through the lipid headgroup region of the neat C_{60} (a), the cationic amino group (b), and the 1-fC_{60} (c), obtained using the adaptive biasing force (ABF) approach. Studied molecules and lipid layer are shown with their real scale. Note different ordinate scale for (b). Insets in (c) show the specific position of 1-fC_{60} corresponding to the barrier at the water/lipid interface and to the energy minimum inside the hydrophobic core of the membrane (see full profile in Figure S2).

about 25 ns) and then proceeds toward the lipid tail region. This shows that monomeric neat C_{60} is able to cross the lipid/water interface, but quite often, fullerenes do aggregate first at the membrane surface. These results confirm previous numerical studies obtained with full atomistic[39] and coarse-grained MD simulations.[33,40] On the other hand, the cationic molecule alone has not shown any propensity to enter the bilayer core (see Figure 2b). Indeed, on the 100 ns time scale, the charged amino derivative stays most of the time in the solvent and, despite occasionally reaching the bilayer headgroup region, does not bind to it strongly (for only 1−4 ns). Hence, the lipid/water interface seems to present a large barrier for translocation of the amino group toward the interior of the membrane. In contrast, when the cationic molecule is conjugated to the fullerene (1-fC_{60} compound), the charged residue penetrates deeper toward the lipid core (see Figure 2c). Several unbiased simulations have indeed shown that 1-fC_{60} crosses the lipid headgroup region. In this process, the amino derivative seems to be dragged toward the middle of the bilayer by the hydrophobic C_{60} moiety.

In order to better quantify the uptake of the three compounds (the C_{60}, the cationic group, and the 1-fC_{60}) by the bilayer, we probed their free-energy profiles as they cross the lipid headgroup interface. The reaction coordinate for fullerene and its derivative was chosen to be the distance between the center of the bilayer and center of mass of the C_{60} sphere and, in the case of the free amino, the distance between its center of the mass and the center of the bilayer. The energy profiles given in Figure 3, estimated using the adaptive biasing force (ABF) method,[41,42] confirm that the hydrophobic nature of the C_{60} favors the uptake of the cationic species by the lipid bilayer. The neat C_{60} displays a large affinity for the lipid tails with an energy well of -8.8 kcal·mol^{-1} (see Figure 3a), and C_{60} uptake is hindered by only a small ($\sim$0.5 kcal·mol^{-1}) energetic barrier. This free-energy profile is in excellent agreement with previous studies.[32,43] In contrast, the cationic group alone (Figure 3b) exhibits no affinity for the membrane since only a small well of -2.2 kcal·mol^{-1} occurs at the membrane's surface. Moreover, the translocation of this molecule, toward the center of the lipid core, requires more than $+25$ kcal·mol^{-1}. The uptake of 1-fC_{60} (Figure 3c) is initially less favored than that of C_{60}, since the compound feels a greater barrier at the entry ($+6.9$ kcal·mol^{-1}). As this barrier is crossed, however, its translocation toward the lipid hydrophobic core seems to be very much favored (-14.2 kcal·mol^{-1}). It is important to mention that due to the conformational freedom of the 1-fC_{60} molecule, the free-energy profile can hardly be estimated accurately along such a simple reaction coordinate (distance between the center of the compound and the center of the bilayer). The convergence of the herein calculated barrier at the lipid/water interface is probably still questionable. During the constrained uptake of 1-fC_{60}, and specifically when reaching the lipid headgroup area, the compound adopts indeed a wide variety of conformations over which it is sampled. Consequently, seen during the MD run the most representative conformation of the compound at the water/lipid interface (see higher inset of Figure 3c) is thus not the only one, which was taken into account during the evaluation of the free-energy barrier. However, the conformation sampled deep within the bilayer corresponds very well to that of the unconstrained MD simulation (see lower inset of Figure 3c). One can then confidently state from the data at hand that the cationic species conjugated to the fullerene is dragged further toward the membrane interior than the bare cationic residue (see Figure 2c.3).

Translocation across the Lipid Tails: Deprotonation Is Needed. Even if the previous calculations show that fullerene enhances the uptake of the cationic group by the lipid bilayer, so far only the translocation of the 1-fC_{60} compound across the lipid headgroup was witnessed. The unconstrained MD simulations of the 1-fC_{60} compound indicate, in agreement with the results from the free-energy estimates (Figure S2), that the amino group remains strongly bound to the lipid heads once the

fullerene, to which the functionalization is attached, has penetrated the core of the membrane (Figure 2c.3). These results contrast with experiment since *n*-fC$_{60}$ and compounds like it have been shown to cross cell membranes under physiological conditions.[32,44,45] The origin of such discrepancy lies probably in the fact that we have considered translocation of the protonated form of the amino group (stable form in solution under normal pH conditions). Recent theoretical studies based on local pK_a measurements and evaluation of the partitioning of amino acid side chains into lipid bilayers indicate however that it is reasonable to expect that some titrable residues (once in the membrane) may change their protonation state after crossing the charged lipid/water interface.[46,47] Such is the case for instance for the Lys residue, which is shown to have a high probability of changing its state from charged to neutral at ~4 Å from the membrane center. Other charged residues such as acidic Asp and Glu are found to be neutral already in the carbonyl group region! (more than 16 Å from the center of the POPC membrane). Other investigations also considered that a negative shift in local pK_a can occur once the positively charged bases are stabilized in the lipid environment, which importantly increases the probability of losing their charge in favor of a neutral form.[48,49]

In order to check if deprotonation of the amino derivative occurs when the cationic group is located in the headgroup region, one needs to estimate its local pK_a. To our knowledge, there are no experimental pK_a values for *n*-amino-fC$_{60}$ derivatives. As the first approximation, we considered the monoethanolammonium ion (HO(CH$_2$)$_2$-NH$_3^+$) as a good model of the cationic group, which can be treated as independent of the C$_{60}$ core considered in the present study. The pK_a of the monoethanolammonium ion amounts to 9.5 under neutral pH.[50] This corroborates the fact that the protonated state is dominant in the aqueous phase. We then consider dissociation of the proton from the charged amino group taking place in the vicinity of the negatively charged phosphorus of the lipid headgroup, *i.e.*, the location where the amino group is trapped (Figure 2c.3). The lipid headgroups can be modeled in two ways depending on the desired degree of complexity (see Supporting Information for more details). The simplest approach is to consider the dihydrogen phosphate ion ($H_2PO_4^-$) as a model system of the nearest negatively charged phosphorus. Reaction of H_3PO_4 dissociation to $H_2PO_4^-$ has a pK_a value equal to 2.12.[51] A more complicated, yet more realistic, approach is to model the lipid headgroup with a whole phosphocholine molecule ($C_5H_{15}NO_4P$). To our knowledge, there is no experimental pK_a value available for this molecule. A predictive pK_a = 6.18 was found for phosphocholine using the Marvin ChemAxon software. As a consequence, one can evaluate the local pK_a of the ethanolammonium ion in these two models of lipid headgroups (see Supporting Information). When we consider $H_2PO_4^-$, the local pK_a for the ethanolammonium ion decreases to 7.38, being very close to the pH under physiological conditions (from 7.2 for cytoplasm to 7.45 for blood).[52] If the pK_a is equal to the pH, an equal probability to have the neutral and ionized form is thus found. This result, even extremely simplified, shows that it is reasonable to consider deprotonation during translocation of cationic species. The second model using a phosphocholine molecule leads to a much more pronounced negative shift of the pK_a for the ethanolammonium ion (~3.32). This means that over 99.9% of amino groups could be already in the neutral form near the lipid headgroups. Even if the second model is based only on the predictive pK_a, it strengthens the deprotonation hypothesis during translocation of the cationic molecules.

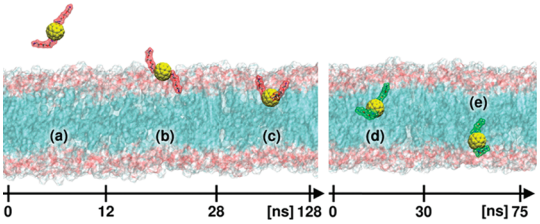

Figure 4. Uptake of a single 2-fC$_{60}$ by POPC membrane (a). Results are from a total of ~200 ns unconstrained MD simulations. This bis-adduct easily crosses the lipid headgroup (b). However, due to strong interactions with lipid heads (c), it needs to be deprotonated in order to fully translocate the membrane (d and e) (see details in the text). Yellow balls indicate the fullerene core with two ionized (red) or neutral (green) amino derivatives. Lipid membrane head and tail sections are shown as red and blue surfaces, respectively. For clarity reasons, water molecules and other mono- and bis-adducts that have not been taken up are not shown.

We have thus taken this into account in the MD simulations of the 1-fC$_{60}$ molecule as shown in Figure 2c. Following the deprotonation of the amino group of the 1-fC$_{60}$ compound (Figure 2c.4), the molecule starts to effectively penetrate the hydrophobic zone of the bilayer, which was unfavorable before. This translocation occurs ~20 ns after the change from the ionized to the neutral form (Figure 2c.5).

Translocation of Multifunctionalized Fullerenes. The number of amino substituents on the C$_{60}$ cage must be chosen carefully in order to ensure the passive diffusion across the lipid headgroups. To quantify the most favorable configuration enabling the relatively easy translocation throughout the lipid bilayer, a MD run of 200 ns of a system containing an equal mixture of 1-fC$_{60}$ and 2-fC$_{60}$ molecules (three mono- and three bis-adducts) was performed. The simulations show that the bis-adduct enters into the membrane core (crosses the lipid headgroup region) within the same time scale as does the monoadduct (see Figure 4). The bis-adduct rapidly passes the lipid headgroup region (within ~28 ns) and remains there for the remainder of the 100 ns simulation; the two amino groups are pinned to the headgroups probably due to favorable electrostatic interactions. Meanwhile, other mono- and bis-adducts aggregate in the bulk water and do not show any specific propensity to go inside the

lipid bilayer (data not shown). As in the previous MD run shown in Figure 2c, when the monomeric species is trapped at the membrane interface, complete translocation is not fully observed. After 128 ns, following the deprotonation hypothesis, we switched the amino groups of the bis-adduct that partially translocated to the membrane core to its neutral form (see Figure 4d). Consequently, within the next 75 ns, it spontaneously migrates toward the other leaflet of the membrane (Figure 4e). To further quantify the influence of the number of cationic residues on the C_{60} cage on passive diffusion, we evaluated the free-energy profiles of three compounds: 1-fC_{60}, 2-fC_{60}, and 7-fC_{60} (see Figures S2, S3, and S4, respectively). The charged species of mono- and bis-adducts show an important energybarrier located deeper in the membrane, which is directly linked to the amino groups that pin to the lipid heads. In the case of their neutral forms, the flat shape of the energy profile confirms their ability to easily cross the hydrophobic part of the membrane, in agreement with the performed unconstrained MD simulation results. In the case of 7-fC_{60}, the uptake is clearly unfavorable since the energy barrier continuously rises from the solvent toward the membrane center up to $+80$ kcal·mol^{-1}. Bearing seven cationic amino derivatives, the 7-fC_{60} is much larger than the mono- and bis-adduct. More importantly, such an amount of the amino derivatives appears to completely screen the lipophilic fullerene core, as the C_{60} can no longer play the role of membrane insertion enhancer. Due to a large number of amino derivatives, the molecule remains in contact with the bulk solvent, and accordingly, it is not appropriate to consider here deprotonation of the cationic groups. This result strongly suggests that if the compounds such as 7-fC_{60} could still penetrate cell membranes, they would probably take another pathway, such as endocytosis. Precise estimation of the cut off, concerning the favorable amount of amino derivatives, still being dragged by C_{60} toward the membrane center, will be the subject of further study.

Insertion and Release Rates. The results presented so far show how and when C_{60} and fC_{60} may insert in the core of the POPC membrane. In order to extract the macroscopic data concerning the permeation of fC_{60} molecules, we have built a simple one-dimensional model inspired by the single-state molecular motor theory.[53] Assuming optimal conditions for protonation/deprotonation of the amino groups exist at the water/lipid interface, we can estimate the insertion and release rates using a stochastic model described in the Methods section, in which the particles diffuse under the action of the MD-derived free-energy profiles. For C_{60} as well as for the charged species 1-fC_{60} and 2-fC_{60}, we found that the molecules are only inserted in the membrane (data not shown). When the deprotonation mechanism is included, we found that 1-fC_{60} and 2-fC_{60} can translocate through the whole bilayer (see Figure S5). The insertion and release rates, namely, $\theta_I(t)$ and $\theta_R(t)$, exhibit an exponential behavior (see Figure S6), and the results of the model show a significant difference in the corresponding characteristic times for insertion τ_I and release τ_R between the two compounds. The estimated rates are respectively $\tau_I = 1.53$ ms and $\tau_R = 1.57$ ms for 1-fC_{60} and $\tau_I = 27.27\ \mu$s and $\tau_R = 28.06\ \mu$s for 2-fC_{60}. For 7-fC_{60}, τ_I and τ_R tend obviously to infinity, which means that this molecule cannot be passively taken up. The net flux of 2-fC_{60} expressed here for the charged species in pA ($I = 6.5$ pA) is about 2 orders of magnitude larger than that obtained for 1-fC_{60} ($I = 0.1$ pA).

CONCLUSIONS

Extensive MD simulations and free-energy calculations have been conducted in order to investigate the interaction of amino derivatives and functionalized fullerenes fC_{60} with model cell membranes. The results show that the fullerene is a good vector that helps the cationic groups (which are not taken up alone) to translocate across the lipid/water interface. Following such translocation, the nature of the charged amino head of the amino derivative favors its strong binding to the lipid headgroups. Meanwhile, the other side of the derivative is dragged toward the bilayer center by the fullerene. Deprotonation of the charged amino head favors full translocation of the fC_{60} compound toward the other bilayer leaflet. Such a deprotonation appears to be in fact necessary for the full permeation of the compound. The lipid bilayer is however very selective with respect to the amount of amino groups conjugated with C_{60}. The ABF profiles show that the uptake mechanism of the n-fC_{60} (n = 1, 2, 7) amino adducts result from a subtle balance involving a repulsive (steric and electrostatic) effect between the fC_{60} and the lipids and the attractive (hydrophobic and lipophilic) character of the C_{60} cage (see Figures S7, S8, and S9). As a result, transferring the 7-fC_{60} fullerene from bulk water into the lipid bilayer is highly unfavorable, while the mono- and bis-adduct are able to passively diffuse toward the hydrophobic part of the membrane. Hence, the fullerene core is shown to enhance intracellular internalization of charged species bearing a reasonable amount of cationic groups.

METHODS

Unconstrained full atomistic MD simulations were performed on neat C_{60} and on amino-C_{60} fullerene derivatives in the vicinity of a fully hydrated palmitoyl-oleyl-phosphatidyl-choline bilayer. The translocation energy profiles of C_{60} fullerene and fC_{60} amino derivatives from bulk water toward to the

membrane center was determined using the adaptive biasing force approach.[41]

We considered the following molecular systems:

(i) Neat C_{60}: Two separate systems were used. The first one was used for the free-energy calculations and contained one C_{60} fullerene interacting with a POPC lipid bilayer composed of 72 molecules. The system was hydrated with 3689 water molecules (total of 16 455 atoms in a volume of $48 \times 40 \times 103$ Å^3). The second system used for MD simulations was composed of four neat C_{60} carbon fullerene molecules, a fully hydrated POPC membrane patch of 180 lipid molecules, and 11 830 water molecules (total system of 49 050 atoms, vol. $68 \times 72 \times 116$ Å^3, total simulation time of 100 ns).

(ii) C_{60} with one amino derivative: Two separate sets were performed. For the free-energy calculation, the system was composed of one C_{60} carbon fullerene molecule to which one charged amino derivative was grafted (monoadduct), a membrane patch of 72 POPC lipid molecules, and 3671 water molecules (total of 16 433 atoms in a volume of $40 \times 51 \times 96$ Å^3). To ensure the electroneutrality of the system, one chloride ion was added. For the unconstrained MD simulations, the system was composed of three monoadducts placed initially near a 180 POPC lipid molecule membrane patch ($70 \times 75 \times 109$ Å^3), hydrated with 11 801 water molecules, and three chloride counterions. Deprotonation (after a 30 ns run) was performed simply by deletion of one hydrogen on the head of the amino derivative (the partial charge was compensated on the nitrogen atom in order to obtain the electroneutrality, which is in very good accordance with the quantum calculations (data not shown)). The counterion was also deleted from the system.

(iii) C_{60} with two amino derivatives: Two independent systems were considered. For the ABF free-energy evaluation, the system was composed of one C_{60} carbon fullerene molecule to which two charged amino derivatives were grafted (bis-adduct), a 72 POPC lipid molecule membrane patch, 3650 water molecules, and two chloride counterions (total of 16 402 atoms in a volume of $46 \times 46 \times 93$ Å^3). For MD simulations, the numerical system contained three bis-adducts and three monoadducts placed initially near the 180 POPC lipid molecule membrane patch (total system of $70 \times 75 \times 109$ Å^3, 11 576 water molecules, nine chloride counterions, total simulation time of 200 ns). The deprotonation of the bis-adduct was ensured in the same way as for the monoadduct, and two corresponding counterions were also deleted from the system.

(iv) C_{60} with seven amino derivatives: Only the ABF free-energy calculation was carried out. The system was composed of one C_{60} carbon fullerene molecule with seven charged amino derivatives attached, a 72 POPC lipid molecule membrane patch, and 3373 water molecules (total of 16 331 atoms in a volume of $47 \times 42 \times 98$ Å^3). To ensure the electroneutrality of the charged system, seven chloride ions were added.

(v) Amino group: An unconstrained MD simulation and ABF free-energy evaluation were performed. For the ABF analysis, one unconjugated amino group was placed in the vicinity of the 72 POPC lipid molecule membrane bilayer hydrated with 3697 water molecules and one chloride counterion (total of 16 457 atoms in a volume of $45 \times 48 \times 89$ Å^3). The MD run was executed during 100 ns on the same system as used for the free-energy evaluation.

Molecular Dynamics Method. The MD simulations were performed using NAMD software.[54] They were conducted at a constant temperature of 300 K (Langevin dynamics) and a constant pressure of 1 atm using the Langevin piston Nosé-Hoover method.[55] Short- and long-range forces were calculated every one and two time steps, respectively, with a time step of 2.0 fs. Chemical bonds between hydrogen and heavy atoms were constrained to their equilibrium values. Long-range electrostatic forces were evaluated using the particle mesh Ewald method.[56]

All systems were modeled using the CHARMM27[57] force field with a united atoms representation for the acyl chains of the lipid molecules. No charges were attributed to the C_{60} carbon (C) atoms, and for fullerene C−C or fullerene C−water oxygen (O) interactions we used the Bedrov *et al.*[58,59] Lennard-Jones potential parameters (CHARMM27 functional: $\sigma_{CC} = 3.895$ Å, $\varepsilon_{CC} = 0.066$ kcal·mol^{-1} and $\sigma_{CO} = 3.58$ Å, $\varepsilon_{CO} = 0.0936$ kcal·mol^{-1}). Water molecules were treated within the TIP3P model.[60] For the potential parameters of the amino group, we followed the general procedure described by Norrby and Brandt,[61] and we performed the *ab initio* quantum calculations using Gaussian 03 package software.[62] The geometrical optimization of a single amino group was performed using the Hartree−Fock approach. The split-valence 6-31+G basis set was employed for all atoms, and obtained Mulliken partial charges were applied to the molecular model.[63]

Adaptive Biasing Force Method. The free-energy profiles were performed using NAMD software[54] with the ABF extensions integrated in the Collective Variables module[64] and under the same conditions as described for MD simulations. The minimal sampling was equal to 100 000 samples for each step along the reaction coordinate, taken as a distance between center of mass (COM) of the fullerene core and the COM of the lipid bilayer along the *z* axis, with a step of 0.1 Å. In the case of the amino group itself, the reaction coordinate was chosen as a distance along the bilayer normal (*z* axis) between the COM of the amino group and the COM of the lipid bilayer, with the same step of 0.1 Å.

Stochastic Model. In this model, the individual molecules can diffuse according to the Smoluchowski equation in the effective potential deduced from the MD simulations. Let us assume that the system contains *N* molecules located initially in the external side of the membrane (say left) and that their motion is restricted to the direction *z* perpendicular to the membrane surface with imposed boundaries of −40 and 40 Å. Using a discrete description of the position ($z = n\Delta z$ with a Δz step of 1 Å), the probability $p(z, t) \approx p(n, t)$ that a given molecule is located at position *z* at a given time *t* obeys the following equation:

$$\begin{aligned} p(n, t+\Delta t) = {} & p(n, t) + k(n+1)W(n+1, n)p(n+1, t)\Delta t \\ & + k(n-1)W(n-1, n)p(n-1, t)\Delta t \\ & - k(n)W(n, n+1)p(n, t)\Delta t \\ & - k(n)W(n, n-1)p(n, t)\Delta t \end{aligned} \quad (1)$$

where $k(i)$ is the attempt frequency, which is closely related to the second derivative of *G* at site *i*, and $W(i, j)$ represents the probability for the particle to jump from position *i* to position *j*. $W(i, j)$ is related to *G* and the thermal energy k_bT (k_b is the Boltzmann constant) through a simple Arrhenius law:

$$W(i, j) \propto e^{(-[G(j) - G(i)]/k_bT)} \quad (2)$$

Note that only jumps from adjacent positions are allowed here.

The integration of eq 1 for different sets of time and positions can be easily performed assuming initial conditions of $p(-40,0) = N$. The insertion and release rates, $\theta_I(t)$ and $\theta_R(t)$, respectively, were calculated by considering the number of particles crossing the left and right sides of the membrane. The flux across the membrane was defined as

$$I(t) = \frac{\Delta\theta_R(t)}{\Delta t} q \quad (3)$$

(expressed in pA) where *q* is the charge carried by *n*-fC_{60}.

Provided the two energy profiles for each molecule corresponding to the charged and neutral form of cationic residues, the effective potential was constructed as follows: the protonated profile was used for molecules located outside the membrane, while the deprotonated one was considered for the molecules located inside the membrane. The switching distance was fixed for each molecule and was derived directly from MD observations, *i.e.*, ±19, ±11, and ±19 Å for 1-fC_{60}, 2-fC_{60}, and 7-fC_{60}, respectively. Since compound 7-fC_{60} was not

evaluated using unconstrained MD, we adopted the highest value of location where the deprotonation can occur, *i.e.*, those of the 1-fC_{60} molecule.

Acknowledgment. The authors wish to thank F. Obert for the fruitful discussion on the chemical aspects of the pK_a, and S. Yasothornsrikul for the critical review of the manuscript. The authors were granted access to the HPC resources of the Mésocentre, a regional computational center at the University of Franche-Comté, and of the Centre Informatique National de l'Enseignement Supérieur (CINES) under the allocations 2009- and 2010-075136 made by GENCI (Grand Equipement National de Calcul Intensif).

Supporting Information Available: Discussion on the local pK_a shift for amino groups in the hydrophilic part of the bilayer is presented. Free-energy profiles, results from the stochastic model, and force profiles acting on charged and neutral forms of studied fC_{60} compounds are also shown. This material is available free of charge *via* the Internet at http://pubs.acs.org.

REFERENCES AND NOTES

1. Riehemann, K.; Schneider, S. W.; Luger, T. A.; Godin, B.; Ferrari, M.; Fuchs, H. Nanomedicine-Challenge and Perspectives. *Angew. Chem., Int. Ed.* **2009**, *48*, 872–897.
2. Caruthers, S. D.; Wickline, S. A.; Lanza, G. M. Nanotechnological Applications in Medicine. *Curr. Opin. Biotechnol.* **2007**, *18*, 26–30.
3. Jain, K. K. Role of Nanobiotechnology in the Development of Personalized Medicine. *Nanomedicine* **2009**, *4*, 249–252.
4. Torchilin, V. P. Multifunctional Nanocarriers. *Adv. Drug Delivery Rev.* **2006**, *58*, 1532–1555.
5. Gregoriadis, G. *Liposomes as Drug Carriers: Recent Trends and Progress*; John Wiley & Sons: New York, 1988.
6. Rolland, A. *Pharmaceutical Particulate Carriers*; Marcel Dekker: New York, 1993.
7. Nishiyama, N.; Kataoka, K. Current State, Achievements, and Future Prospects of Polymeric Micelles as Nanocarriers for Drug and Gene Delivery. *Pharmacol. Ther.* **2006**, *112*, 630–648.
8. Shi, X. Y.; Thomas, T. P.; Myc, L. A.; Kotlyar, A.; Baker, J. R. Synthesis, Characterization, and Intracellular Uptake of Carboxyl-Terminated Poly(Amidoamine) Dendrimer-Stabilized Iron Oxide Nanoparticles. *Phys. Chem. Chem. Phys.* **2007**, *9*, 5712–5720.
9. Lal, S.; Clare, S. E.; Halas, N. J. Nanoshell-Enabled Photothermal Cancer Therapy: Impending Clinical Impact. *Acc. Chem. Res.* **2008**, *41*, 1842–1851.
10. Klumpp, C.; Kostarelos, K.; Prato, M.; Bianco, A. Functionalized Carbon Nanotubes as Emerging Nanovectors for the Delivery of Therapeutics. *Biochim. Biophys. Acta, Biomembr.* **2006**, *1758*, 404–412.
11. Prato, M.; Kostarelos, K.; Bianco, A. Functionalized Carbon Nanotubes in Drug Design and Discovery. *Acc. Chem. Res.* **2008**, *41*, 60–68.
12. Brettreich, M.; Hirsch, A. A Highly Water-Soluble Dendro [60]Fullerene. *Tetrahedron Lett.* **1998**, *39*, 2731–2734.
13. Brettreich, M.; Burghardt, S.; Bottcher, C.; Bayerl, T.; Bayerl, S.; Hirsch, A. Globular Amphiphiles: Membrane-Forming Hexaadducts of C-60. *Angew. Chem., Int. Ed.* **2000**, *39*, 1845–1848.
14. Burghardt, S.; Hirsch, A.; Schade, B.; Ludwig, K.; Bottcher, C. Switchable Supramolecular Organization of Structurally Defined Micelles Based on an Amphiphilic Fullerene. *Angew. Chem., Int. Ed.* **2005**, *44*, 2976–2979.
15. Partha, R.; Conyers, J. L. Biomedical Applications of Functionalized Fullerene-Based Nanomaterials. *Int. J. Nanomed.* **2009**, *4*, 261–275.
16. Da Ros, T.; Prato, M. Medicinal Chemistry with Fullerenes and Fullerene Derivatives. *Chem. Commun.* **1999**, 663–669.
17. Ruoff, R. S.; Tse, D. S.; Malhotra, R.; Lorents, D. C. Solubility of C60 in a Variety of Solvents. *J. Phys. Chem.* **1993**, *97*, 3379–3383.
18. Sivaraman, N.; Dhamodaran, R.; Kaliappan, I.; Srinivasan, T. G.; Rao, P. R. V.; Mathews, C. K. Solubility of C60 in Organic Solvents. *J. Org. Chem.* **1992**, *57*, 6077–6079.
19. Noon, W. H.; Kong, Y. F.; Ma, J. P. Molecular Dynamics Analysis of a Buckyball-Antibody Complex. *Proc. Natl. Acad. Sci. U. S. A.* **2002**, *99*, 6466–6470.
20. Zhao, X. C.; Striolo, A.; Cummings, P. T. C-60 Binds to and Deforms Nucleotides. *Biophys. J.* **2005**, *89*, 3856–3862.
21. Friedman, S. H.; Decamp, D. L.; Sijbesma, R. P.; Srdanov, G.; Wudl, F.; Kenyon, G. L. Inhibition of the Hiv-1 Protease by Fullerene Derivatives—Model-Building Studies and Experimental-Verification. *J. Am. Chem. Soc.* **1993**, *115*, 6506–6509.
22. Sijbesma, R.; Srdanov, G.; Wudl, F.; Castoro, J. A.; Wilkins, C.; Friedman, S. H.; Decamp, D. L.; Kenyon, G. L. Synthesis of a Fullerene Derivative for the Inhibition of HIV Enzymes. *J. Am. Chem. Soc.* **1993**, *115*, 6510–6512.
23. Sayes, C. M.; Fortner, J. D.; Guo, W.; Lyon, D.; Boyd, A. M.; Ausman, K. D.; Tao, Y. J.; Sitharaman, B.; Wilson, L. J.; Hughes, J. B.; *et al*. The Differential Cytotoxicity of Water-Soluble Fullerenes. *Nano Lett.* **2004**, *4*, 1881–1887.
24. Sayes, C. M.; Gobin, A. M.; Ausman, K. D.; Mendez, J.; West, J. L.; Colvin, V. L. Nano-C-60 Cytotoxicity Is Due to Lipid Peroxidation. *Biomaterials* **2005**, *26*, 7587–7595.
25. Mashino, T.; Nishikawa, D.; Takahashi, K.; Usui, N.; Yamori, T.; Seki, M.; Endo, T.; Mochizuki, M. Antibacterial and Antiproliferative Activity of Cationic Fullerene Derivatives. *Bioorg. Med. Chem. Lett.* **2003**, *13*, 4395–4397.
26. Aoshima, H.; Kokubo, K.; Shirakawa, S.; Ito, M.; Yamana, S.; Oshima, T. Antimicrobial Activity of Fullerenes and Their Hydroxylated Derivatives. *Biocontrol Sci.* **2009**, *14*, 69–72.
27. Yacoby, I.; Benhar, I. Antibacterial Nanomedicine. *Nanomedicine* **2008**, *3*, 329–341.
28. Partha, R.; Mitchell, L. R.; Lyon, J. L.; Joshi, P. P.; Conyers, J. L. Buckysomes: Fullerene-Based Nanocarriers for Hydrophobic Molecule Delivery. *ACS Nano* **2008**, *2*, 1950–1958.
29. Dugan, L. L.; Turetsky, D. M.; Du, C.; Lobner, D.; Wheeler, M.; Almli, C. R.; Shen, C. K. F.; Luh, T. Y.; Choi, D. W.; Lin, T. S. Carboxyfullerenes as Neuroprotective Agents. *Proc. Natl. Acad. Sci. U. S. A.* **1997**, *94*, 9434–9439.
30. Cusan, C.; Da Ros, T.; Spalluto, G.; Foley, S.; Janto, J. M.; Seta, P.; Larroque, C.; Tomasini, M. C.; Antonelli, T.; Ferraro, L.; *et al*. A New Multi-Charged C-60 Derivative: Synthesis and Biological Properties. *Eur. J. Org. Chem.* **2002**, 2928–2934.
31. Bosi, S.; Da Ros, T.; Spalluto, G.; Balzarini, J.; Prato, M. Synthesis and Anti-HIV Properties of New Water-Soluble Bis-Functionalized[60]Fullerene Derivatives. *Bioorg. Med. Chem. Lett.* **2003**, *13*, 4437–4440.
32. Qiao, R.; Roberts, A. P.; Mount, A. S.; Klaine, S. J.; Ke, P. C. Translocation of C-60 and Its Derivatives across a Lipid Bilayer. *Nano Lett.* **2007**, *7*, 614–619.
33. D'Rozario, R. S. G.; Wee, C. L.; Wallace, E. J.; Sansom, M. S. P. The Interaction of C-60 and Its Derivatives with a Lipid Bilayer *via* Molecular Dynamics Simulations. *Nanotechnology* **2009**, *20*, 115102.
34. Carr, R.; Weinstock, I. A.; Sivaprasadarao, A.; Muller, A.; Aksimentiev, A. Synthetic Ion Channels *via* Self-Assembly: A Route for Embedding Porous Polyoxometalate Nanocapsules in Lipid Bilayer Membranes. *Nano Lett.* **2008**, *8*, 3916–3921.
35. Kostarelos, K.; Lacerda, L.; Pastorin, G.; Wu, W.; Wieckowski, S.; Luangsivilay, J.; Godefroy, S.; Pantarotto, D.; Briand, J. P.; Muller, S.; *et al*. Cellular Uptake of Functionalized Carbon Nanotubes is Independent of Functional Group and Cell Type. *Nat. Nanotechnol.* **2007**, *2*, 108–113.
36. Pantarotto, D.; Singh, R.; McCarthy, D.; Erhardt, M.; Briand, J. P.; Prato, M.; Kostarelos, K.; Bianco, A. Functionalized Carbon Nanotubes for Plasmid DNA Gene Delivery. *Angew. Chem., Int. Ed.* **2004**, *43*, 5242–5246.
37. Lacerda, L.; Pastorin, G.; Gathercole, D.; Buddle, J.; Prato, M.; Bianco, A.; Kostarelos, K. Intracellular Trafficking of Carbon Nanotubes by Confocal Laser Scanning Microscopy. *Adv. Mater.* **2007**, *19*, 1480–1484.
38. Lacerda, L.; Pastorin, G.; Gathercole, D.; Buddle, J.; Prato, M.; Bianco, A.; Kostarelos, K. Intracellular Trafficking of Carbon Nanotubes by Confocal Laser Scanning Microscopy (Vol 18, Pg 1480, 2007). *Adv. Mater.* **2007**, *19*, 1789–1789.

39. Kraszewski, S.; Tarek, M.; Treptow, W.; Ramseyer, C. Affinity of C-60 Neat Fullerenes with Membrane Proteins: A Computational Study on Potassium Channels. *ACS Nano* **2010**, *4*, 4158–4164.
40. Wong-Ekkabut, J.; Baoukina, S.; Triampo, W.; Tang, I. M.; Tieleman, D. P.; Monticelli, L. Computer Simulation Study of Fullerene Translocation through Lipid Membranes. *Nat. Nanotechnol.* **2008**, *3*, 363–368.
41. Darve, E.; Rodriguez-Gomez, D.; Pohorille, A. Adaptive Biasing Force Method for Scalar and Vector Free Energy Calculations. *J. Chem. Phys.* **2008**, *128*, 144120(13pp).
42. Hénin, J.; Chipot, C. Overcoming Free Energy Barriers Using Unconstrained Molecular Dynamics Simulations. *J. Phys. Chem.* **2004**, *121*, 2904–2914.
43. Li, L. W.; Davande, H.; Bedrov, D.; Smith, G. D. A Molecular Dynamics Simulation Study of C-60 Fullerenes inside a Dimyristoylphosphatidylcholine Lipid Bilayer. *J. Phys. Chem. B* **2007**, *111*, 4067–4072.
44. Andreev, I. M.; Romanova, V. S.; Petrukhina, A. O.; Andreev, S. M. Amino-Acid Derivatives of Fullerene C-60 Behave as Lipophilic Ions Penetrating through Biomembranes. *Phys. Solid State* **2002**, *44*, 683–685.
45. Foley, S.; Crowley, C.; Smaihi, M.; Bonfils, C.; Erlanger, B. F.; Seta, P.; Larroque, C. Cellular Localisation of a Water-Soluble Fullerene Derivative. *Biochem. Biophys. Res. Commun.* **2002**, *294*, 116–119.
46. MacCallum, J. L.; Bennett, W. F. D.; Tieleman, D. P. Partitioning of Amino Acid Side Chains into Lipid Bilayers: Results from Computer Simulations and Comparison to Experiment. *J. Gen. Physiol.* **2007**, *129*, 371–377.
47. Yoo, J.; Cui, Q. Does Arginine Remain Protonated in the Lipid Membrane? Insights from Microscopic pK(a) Calculations. *Biophys. J.* **2008**, *94*, L61–L63.
48. Fernandez, M. S.; Fromherz, P. Lipoid pH Indicators as Probes of Electrical Potential and Polarity in Micelles. *J. Phys. Chem.* **1977**, *81*, 1755–1761.
49. Beschiaschvili, G.; Seelig, J. Peptide Binding to Lipid Bilayers. Nonclassical Hydrophobic Effect and Membrane-Induced pK Shifts. *Biochemistry* **1992**, *31*, 10044–10053.
50. Hall, H. K. Correlation of the Base Strengths of Amines. *J. Am. Chem. Soc.* **1957**, *79*, 5441–5444.
51. McMurry, J. E.; Fay, R. C. *Chemistry*, 4th ed.; Prentice-Hall, Inc.: NJ, 2004.
52. Boron, W.; Boulpaep, E. *Medical Physiology: A Cellular and Molecular Approach*, 2d ed.; Elsevier Saunders: Portland, OR, 2009; p 1337.
53. Aksimentiev, A.; Balabin, I. A.; Fillingame, R. H.; Schulten, K. Insights into the Molecular Mechanism of Rotation in the F_o Sector of ATP Synthase. *Biophys. J.* **2004**, *86*, 1332–1344.
54. Phillips, J. C.; Braun, R.; Wang, W.; Gumbart, J.; Tajkhorshid, E.; Villa, E.; Chipot, C.; Skeel, R. D.; Kale, L.; Schulten, K. Scalable Molecular Dynamics with Namd. *J. Comput. Chem.* **2005**, *26*, 1781–1802.
55. Feller, S. E.; Zhang, Y. H.; Pastor, R. W.; Brooks, B. R. Constant-Pressure Molecular-Dynamics Simulation—the Langevin Piston Method. *J. Chem. Phys.* **1995**, *103*, 4613–4621.
56. Darden, T.; York, D.; Pedersen, L. Particle Mesh Ewald: An N. Log(N) Method for Ewald Sums in Large Systems. *J. Chem. Phys.* **1993**, *98*, 10089–10092.
57. MacKerell, A. D.; Bashford, D.; Bellott, M.; Dunbrack, R. L.; Evanseck, J. D.; Field, M. J.; Fischer, S.; Gao, J.; Guo, H.; Ha, S.; *et al*. All-Atom Empirical Potential for Molecular Modeling and Dynamics Studies of Proteins. *J. Phys. Chem. B* **1998**, *102*, 3586–3616.
58. Bedrov, D.; Smith, G. D.; Davande, H.; Li, L. W. Passive Transport of C-60 Fullerenes through a Lipid Membrane: A Molecular Dynamics Simulation Study. *J. Phys. Chem. B* **2008**, *112*, 2078–2084.
59. Li, L. W.; Bedrov, D.; Smith, G. D. Water-Induced Interactions between Carbon Nanoparticles. *J. Phys. Chem. B* **2006**, *110*, 10509–10513.
60. Jorgensen, W. L.; Chandrasekhar, J.; Madura, J. D.; Impey, R. W.; Klein, M. L. Comparison of Simple Potential Functions for Simulating Liquid Water. *J. Chem. Phys.* **1983**, *79*, 926–935.
61. Norrby, P. O.; Brandt, P. Deriving Force Field Parameters for Coordination Complexes. *Coord. Chem. Rev.* **2001**, *212*, 79–109.
62. Frisch, M. J.; Trucks, G. W.; Schlegel, H. B.; Scuseria, G. E.; Robb, M. A.; Cheeseman, J. R.; Montgomery, J. A.; Vreven, J., T. ; Kudin, K. N.; Burant, J. C.; *et al*. *Gaussian 03*, Rev. C.02; Gaussian, Inc.: Wallingford, CT, 2004.
63. Mulliken, R. S. Electronic Population Analysis on LCAO-MO Molecular Wave Functions 1. *J. Chem. Phys.* **1955**, *23*, 1833–1840.
64. Henin, J.; Fiorin, G.; Chipot, C.; Klein, M. L. Exploring Multidimensional Free Energy Landscapes Using Time-Dependent Biases on Collective Variables. *J. Chem. Theory Comput.* **2010**, *6*, 35–47.